β-Turn Phe in HIV-1 Env Binding Site of CD4 and CD4 Mimetic Miniprotein Enhances Env Binding Affinity but Is Not Required for Activation of Co-Receptor/17b Site

Cynthia S. Dowd,[‡] Stephanie Leavitt,[§] Gregory Babcock,[||] Alexis P. Godillot, Don Van Ryk, Gabriela A. Canziani, Joseph Sodroski,[||] Ernesto Freire,[§] and Irwin M. Chaiken*

Department of Medicine, University of Pennsylvania, Philadelphia, Pennsylvania 19104, Department of Biology, The Johns Hopkins University, Baltimore, Maryland 21218, and Department of Cancer Immunology and AIDS, Dana-Farber Cancer Institute and Division of AIDS, Harvard Medical School, Boston, Massachusetts 02115

Received December 18, 2001; Revised Manuscript Received March 13, 2002

ABSTRACT: HIV-1 enters a host cell after an initial interaction between viral envelope glycoprotein gp120 and cell surface receptor CD4, followed by a second interaction between gp120 and a cell surface chemokine receptor. CD4 residue Phe43 makes a significant contribution to the high-affinity interaction between CD4 and env. We and others have used scorpion toxin scaffolds to display and examine CD4 epitopes used for gp120 recognition. These peptides, which have a β-turn Phe that acts as a Phe43 surrogate, compete with CD4 for gp120 binding and enhance the binding of gp120 to 17b, an antibody that binds near the co-receptor-binding site. In the current study, a scyllatoxin-scaffolded peptide, identified via phage epitope randomization and lacking a β-turn Phe (indeed, containing no aromatic residues), was shown to behave in a distinctly CD4-like manner. This peptide, denoted [$_{20}$EGLV$_{23}$]ST, not only competed with CD4 for gp120 binding, but also enhanced the binding of gp120 to 17b. Quantitatively, an [$_{20}$EGLV$_{23}$]ST-gp120 complex exhibited the same 17b binding on-rate as a complex of gp120 with [$_{20}$AGSF$_{23}$]ST, a scyllatoxin-based CD4 mimetic peptide containing a β-turn Phe. In view of this result, we examined the role of Phe43 in CD4 itself by comparing F43V D1D2 sCD4 versus D1D2 sCD4. Like the peptides, a close similarity was observed for both Phe43 and Phe43-less D1D2 sCD4s in enhancing gp120 binding to 17b. Further, when examined for their ability to enhance binding of gp120 to CCR5$^+$ cells, [$_{20}$EGLV$_{23}$]ST and [$_{20}$AGSF$_{23}$]ST were found to have the same efficacy, after correcting for the difference in their gp120 affinities. These results show that, although Phe43 is important in maintaining high affinity in gp120 ligands, the aromatic residue is not necessary for triggering the conformational isomerization in gp120 that results in formation or exposure of the binding sites for the 17b antibody and the CCR5 receptor.

Infection of a host cell by the human immunodeficiency virus (HIV-1),[1] the virus that causes AIDS (*1*), is initiated by key binding events between the cell and the viral particle. Initially, gp120, the HIV-1 surface envelope glycoprotein, binds to CD4, a receptor on the host cell surface. This binding leads to a conformational change that exposes a second binding site on an adjacent face of gp120 (*2*, *3*) that is used to bind to a second host cell surface receptor, a chemokine receptor. Triggered by these two binding events, the transmembrane envelope glycoprotein, gp41, is thought to become exposed. Once gp41 reorganizes into a fusogenic conformation, membrane fusion between HIV-1 and the host cell occurs and infection proceeds. From this current view, it is clear that understanding the mechanisms of gp120-CD4 and gp120-chemokine receptor interactions would provide insights into the process of HIV-1 entry and, in turn, the design of HIV-1 entry inhibitors.

The chemokine receptors CCR5 and CXCR4 are the major secondary receptors used by HIV-1 to bind to the cell surface (*4*−*10*). By mutagenesis, structural analysis, and epitope mapping studies, the binding sites for CCR5 and CXCR4 on gp120 have been identified (*11*, *12*). From these studies, the binding site of an antibody, 17b, was found to overlap with the binding site of the CCR5 receptor on the gp120 surface (*13*). In the same way that gp120 binding to CCR5 is enhanced by the prior binding of CD4, the binding of gp120 to 17b is also increased in the presence of CD4 (*13*). We and others have used 17b binding to gp120, and its enhancement, as a model for gp120-CCR5 receptor binding (*14*).

A crystal structure of gp120 in complex with the first two domains (D1D2) of sCD4 and a 17b Fab fragment has been reported (*15*). D1D2 sCD4 has been shown to have equivalent affinity to gp120 when compared with full-length sCD4

* To whom correspondence should be addressed. Phone: (215) 573-9678. Fax: (215) 349-5572. E-mail: chaiken@mail.med.upenn.edu.
[‡] Present address: Laboratory of Immunogenetics, NIAID, NIH, Rockville, MD 20852.
[§] The Johns Hopkins University.
[||] Harvard Medical School.

[1] Abbreviations: BSA, bovine serum albumin; CT, charybdotoxin; D1D2, domains 1 and 2 of soluble CD4; HIV-1, human immunodeficiency virus type 1; PBS, phosphate-buffered saline; ST, scyllatoxin; TFA, trifluoroacetic acid.

10.1021/bi012168i CCC: $22.00
Published on Web 05/10/2002

(*16*). The crystal structure shows that Phe43 and Arg59 of CD4 contribute a significant number of contacts to the interaction with gp120. Phe43 inserts into a deep hydrophobic cavity in the gp120 core, while Arg59 participates in interactions between CD4 and gp120 outside of this hydrophobic pocket. Replacement of Phe43 and Arg59 with Ala by site-directed mutagenesis decreases affinity to IIIB gp120 by 550- and 10-fold, respectively (*17*). Similarly, optical biosensor analysis has measured a 190-fold decrease in affinity for BH-10 gp120 resulting from a mutation of Phe43 to Val (*16*).

We and others have used peptide scaffolds to display CD4 epitopes that bind to gp120 (*14*, *18*−*21*). One scaffold that has been successfully altered to mimic CD4 is charybdotoxin (CT). CT belongs to a family of scorpion toxins, which are 25−32 residues in length and are characterized by the presence of three disulfide bonds (*22*, *23*). TXM1, a peptide mimetic based on a charybdotoxin scaffold, was found to bind to gp120, compete with sCD4 for gp120 binding, and enhance gp120 binding to 17b (*14*). To gain insight into the structural determinants for binding gp120, TXM1 was used as the basis for a phage display library. The four residues appearing in the β-turn (i.e., QGSF in TXM1) were randomized (*18*). This region corresponds to the β-turn region of CD4 containing Phe43 (i.e., $_{40}$QGSF$_{43}$). The library yielded several peptide sequences that bound to gp120 competitively with sCD4 but, interestingly, did not contain an aromatic residue among the four varied residues.

The dominance of nonaromatic miniprotein selectants evoked the questions to what extent do these molecules recapitulate the binding properties of CD4 and what is the role of the β-turn Phe in envelope interactions. In the current study, we examined the binding properties of the most frequently selected sequence from phage display, EGLV, and the corresponding CD4 D1D2 variant, F43V D1D2. The results clarify the role of Phe43 in HIV-1 entry and may help facilitate the development of HIV-1 entry antagonists.

MATERIALS AND METHODS

Protein Production

The gp120 envelope protein from the CCR5-using, primary HIV-1 strain YU2 was expressed in Drosophila *Schneider 2* (S2) cells as previously described (*24*). The recombinant protein was purified using an affinity column composed of fast-flow Sepharose coated with protein A onto which F105, a high affinity monoclonal antibody, was immobilized. Cell supernatant was passed over the F105 column to capture the expressed gp120. The column was washed with PBS to remove undesired supernatant components, and purified gp120 was eluted using 0.1 M citrate (pH 3.4). Human monoclonal antibody 17b was expressed in human hybridoma cells (*25*) grown in RPMI 1640 media supplemented with 10% fetal calf serum. The antibody was purified by affinity chromatography using a protein A-linked agarose column (LTI, Gaithersburg, MD) and eluted with 100 mM citric acid (pH 3.4). Fab fragments were produced by papain digestion (Pierce) as previously described (*14*). The sCD4 proteins (D1D2 and F43V in the D1D2 construct) were generous gifts from Ray Sweet at SmithKline Beecham Pharmaceuticals.

Peptide Synthesis

[$_{20}$AGSF$_{23}$]ST [=CD4M9 (*19*)] (CNLARCQLRCKSLGLLGKCAGSFCACGP-NH$_2$) and [$_{20}$EGLV$_{23}$]ST (CNLARCQLRCKSLGLLGKCEGLVCACGP-NH$_2$) were synthesized using solid-phase peptide synthesis on an ABI 433A peptide synthesizer (Applied Biosystems, Foster City, CA). The name of each peptide refers to its four-residue sequence in the β-turn hairpin loop.

General Synthetic Procedure. Fmoc-protected amino acids were coupled after activation by 2-(1*H*-Benzotriazol-1-yl)-1,1,3,3-tetramethyluronium hexafluorophosphate (HBTU) and *N*-hydroxybenzotriazole (HOBt). Side-chain protecting groups were trityl (Asn, Cys, Gln), *tert*-butyloxycarbonyl (Lys), *tert*-butyl (Glu, Ser) and 2,2,5,7,8-pentamethylchroman-6-sulfonyl (Arg). Peptides were cleaved from the resin using a mixture of 88.9% TFA, 4.4% ethanedithiol, 4.4% H_2O, and 2.2% thioanisole. The reduced peptides were dissolved in 10% acetic acid/2% dithiothreitol and purified by HPLC on a semipreparative C18 column (Vydac) using a linear gradient (29 to 55% buffer B over 30 min; buffer A = 5% acetonitrile, 0.1% TFA; buffer B = 90% acetonitrile, 0.1% TFA). Following lyophilization, the peptides were oxidized as previously reported (*26*). The oxidized peptides were purified by HPLC using a linear gradient, 20 to 70% buffer B, over 30 min.

Synthetic Details. [$_{20}$AGSF$_{23}$]ST: 0.159 g of rink amide resin was used in a 0.1 mmol synthesis, which resulted in 0.43 g (61.3%) peptide-resin. Cleavage resulted in 0.19 g (66.1 μmol, 35.1%) of dry peptide. Mass spectroscopy of reduced [$_{20}$AGSF$_{23}$]ST gave 2871.5 g/mol (calcd 2872.6). Oxidized [$_{20}$AGSF$_{23}$]ST gave a measured MS value of 2865.3 g/mol (calcd 2866.5). Amino acid analysis (Yale University Keck Facility) was used to determine the final yield of oxidized [$_{20}$AGSF$_{23}$]ST (5.66 mg, 1.97 μmol, 3.0% from reduced peptide or 1.0% from total synthesis). *[$_{20}$EGLV$_{23}$]-ST:* 0.159 g of rink amide resin was used in a 0.1 mmol synthesis, which resulted in 0.57 g (80.7%) of peptide-resin and 0.22 g (75.6 μmol, 40.2%) dry peptide following cleavage. Mass spectroscopy of reduced [$_{20}$EGLV$_{23}$]ST gave 2907.7 g/mol (calcd 2908.6). Oxidized [$_{20}$EGLV$_{23}$]ST gave a measured MS value of 2900.8 g/mol (calcd 2902.6). Amino acid analysis was used to determine the final yield of oxidized [$_{20}$EGLV$_{23}$]ST (11.99 mg, 4.13 μmol, 5.5% from reduced peptide or 2.2% from total synthesis).

Optical Biosensor Binding Assays

General Procedures. Interaction assays were performed on a BIA2000 optical biosensor (Biacore Inc., Upsala Sweden). Immobilization of ligands to a CM5 sensor chip was performed using amine coupling. Briefly, a solution of 0.2 M EDC and 0.05 M NHS was used to activate carboxyl groups on the sensor surface at a flow rate of 5 μL/min for 7 min. The ligand, dissolved in 10 mM NaOAc buffer, pH 5.5, was passed over the sensor chip surface at a flow rate of 5 μL/min until the desired immobilization level was reached. Excess carboxyl groups were capped by injection of 1 M ethanolamine (pH 8.0) at a flow rate of 5 μL/min for 7 min. In all experiments, BSA was immobilized on a neighboring flowcell to act as a reference (nonspecific binding) surface. Prior to all experiments, the binding surfaces were tested with appropriate concentrations of either

gp120 or sCD4 prepared prior to the assay. The sample solutions were mixed at least 1 h prior to injection. All binding experiments were performed in duplicate and at 25 °C. Data points were collected at the highest collection rate (2 Hz).

Peptide Binding to YU2 gp120. gp120 was immobilized to a final surface density of approximately 1500 Response Units (RU). [$_{20}$EGLV$_{23}$]ST and [$_{20}$AGSF$_{23}$]ST solutions were prepared in PBST (PBS + 0.005% Tween 20) plus additional NaCl to a final concentration of 280 mM. Concentrations of 0.094−133.3 μM for [$_{20}$AGSF$_{23}$]ST and 17.6−300 μM for [$_{20}$EGLV$_{23}$]ST were passed over the sensor surface at a flow rate of 30 μL/min for 1 min. Slight differences in NaCl and instrument noise, at the low RU of the responses, were accounted for by subtracting salt-corrected buffer injections from both the BSA and gp120 sensorgrams. The surfaces were regenerated by two 25 μL injections of 6.25 mM NaOH/1 M NaCl at a flow rate of 100 μL/min. Data for [$_{20}$AGSF$_{23}$]ST and [$_{20}$EGLV$_{23}$]ST were analyzed using TableCurve (Jandel Scientific, AISN Software Copyright 1989−1994). The Scatchard plots (in duplicate) were fit using a robust straight line fit to $y = mx + b$ by the least-squares method and a Gaussian distribution of error was used to estimate the standard deviation of the slope. The correlation coefficient r^2 for the fitted straight line was also estimated. K_D estimates are presented as $-1/a \pm$ standard error K_D ($1/\Delta Z \times 1/m$), where ΔZ is the standard error of the slope (m).

F43V (D1D2) sCD4 and D1D2 sCD4 Binding to YU2 gp120. gp120 was immobilized to a final surface density of 500 RU. F43V sCD4 and D1D2 sCD4 solutions were prepared in PBST with 280 mM NaCl. Concentrations of 25−640 nM for F43V sCD4 and 25−320 nM for D1D2 sCD4 were passed over the surface at a flow rate of 30 μL/min for 2 min. Signal differences arising from nonmatching NaCl concentrations due to sample dilution were minimized by subtracting salt-corrected buffer injections from both the BSA and gp120 sensorgrams. The surfaces were regenerated by one 20 μL injection of 10 mM HCl at a flow rate of 100 μL/min.

Competition of sCD4 Binding to gp120 by Peptides. sCD4 (D1−D4) was immobilized to a final surface density of 900 RU. YU2 gp120 (100 nM) and solutions of peptide (39.5−200 μM) plus gp120 (100 nM) were prepared in PBST with 280 mM NaCl and passed over the sensor surface at a flow rate of 30 μL/min for 1 min. Buffer injections were subtracted to correct for buffer artifacts in the sensorgrams. The surfaces were regenerated by one 20 μL injection of 4.5 M $MgCl_2$ followed by one 20 μL injection of 17 mM NaOH/1.3 M NaCl at a flow rate of 100 μL/min.

Effect of Peptides on gp120 Binding to 17b Fab. 17b Fab was immobilized to a final surface density of 600 RU. YU2 gp120 (100 nM) and solutions of peptide (0.025−1.27 μM for [$_{20}$AGSF$_{23}$]ST and 9.2−330 μM for [$_{20}$EGLV$_{23}$]ST) plus gp120 (100 nM) were prepared in PBST with 280 mM NaCl and passed over the sensor surface at a flow rate of 70 μL/min for 1 min. Buffer injections were subtracted to remove any buffer-derived artifacts from the sensorgrams. The surfaces were regenerated by one 20 μL injection of 10 mM HCl at a flow rate of 100 μL/min.

Effect of F43V (D1D2) sCD4 vs D1D2 sCD4 on gp120 Binding to 17b Fab. 17b Fab was immobilized to a final surface density of 400 RU. YU2 gp120 (5 nM) and solutions of sCD4 protein (19.2−1450 nM for F43V or 0.35−11.2 nM for D1D2) plus gp120 (5 nM) were prepared in PBST plus 0.5% soluble carboxymethyldextran and passed over the sensor surface at a flow rate of 70 μL/min for 1 min. Buffer injections were subtracted to remove any artifacts due to the buffer from the sensorgrams. The surfaces were regenerated by one 10 μL injection of 10 μM HCl at a flow rate of 100 μL/min.

Calculation of k_{on} for Binding of Peptide/Protein-gp120 Complexes to 17b Fab. Due to the complexity of the kinetics in the trimolecular interaction, direct fitting of the data (either by global or separate fit) was not attempted. Instead, after buffer and reference surface subtraction from the sample sensorgrams, the association data were averaged and plotted as the change in response/change in time (dR/dt) versus response (R), according to the equation, $dR/dt = k_{on}[A](R_{max} - R) - k_{off}R$. Linear regression was used to find the best-fit line at each concentration. The slopes of these lines correspond to the observed on-rate (k_s), according to the relationship, $k_s = k_{on}[A] + k_{off}$. The on-rates were obtained by plotting the negative k_s ($-k_s$) versus concentration of protein/peptide−gp120 complex. The latter values were found by calculating the percent of complexed gp120 based on the measured affinity (K_D) of gp120 for the protein or peptide. Because the dR/dt plots gave nearly linear relationships with respect to the change in time and secondary plots were linear, the contribution of uncomplexed gp120 to the overall binding observed was treated as negligible.

Isothermal Titration Calorimetric (ITC) Measurements of Affinity of CD4 Mimetic Peptides for YU2 gp120. ITC experiments were performed at 25 °C using a VP−ITC (Microcal, Inc, Northhampton, MA). Experiments were carried out using the following conditions: YU2 gp120 (3.12 μM) titrated with [$_{20}$AGSF$_{23}$]ST (0.05 mM) in Dulbecco's PBS buffer (15.2 mM Na_2HPO_4, 137 mM NaCl, 2.7 mM KCl, 1.5 mM KH_2PO_4, pH 7.4), and YU2 gp120 (18.7 μM) titrated with [$_{20}$EGLV$_{23}$]ST (0.3786 mM) in 10 mM NaH_2PO_4, 200 mM NaCl, 0.5 mM EDTA, pH 7.4. The heat evolved after each injection was obtained from the integral of the calorimetric signal and corrected for the heat of dilution. The data were analyzed using ORIGIN software provided by Microcal. Binding values were obtained using a one-site binding model.

FACS Assay for gp120 Binding to CCR5 Expressing Cells. Measurement of gp120 binding to CCR5+ cells was performed as reported elsewhere (*27*). Briefly, 1×10^6 Cf2Th-CCR5 cells were suspended in 100 μL of PBS supplemented with 5% FCS/0.02% sodium azide. YU2 gp120 (120 ng, 10 nM) was incubated with 1 μg of soluble CD4 or a given concentration of peptide for 1 h at 25 °C and the complexes added to the cells. Incubation proceeded for 1 additional hour at 37 °C. One microgram of C11 anti-gp120 antibody was added and incubated for 45 min at 37 °C. Cells were then pelleted, washed once in PBS supplemented with 5% FCS, and resuspended in 95 μL of PBS/5% FCS containing 5 μL of goat-α-human IgG-PE (Jackson ImmunoResearch). (The IgG was bound to phycoerythrin (PE), which acts as a fluorochrome to identify stained cells.) Reactions were incubated for 20 min at 4 °C, after which the cells were washed two times in PBS/0.5% BSA. Samples

were analyzed using a Becton Dickinson FACScan with CellQuest software.

RESULTS

CD4 Mimetic Peptide Synthesis. Peptides with sequences derived from the charybdotoxin (CT) phage display library (*18*) initially were synthesized in the CT scaffold via solid-phase peptide synthesis. These syntheses typically gave low yields during linear synthesis and multiple products upon oxidation of the disulfide bonds. For these reasons, it was desired to import the selected sequences from the library into a scyllatoxin (ST) scaffold, which gives higher synthetic yields and purity after both linear synthesis and oxidation. In the initial stage of this work, we examined the effect of transferring a phage-selected sequence from the CT scaffold to the ST scaffold on gp120 binding using the previously studied selectant, GQTL (*18*). Transfer of sequences from the CT to ST scaffold resulted in no loss of affinity for gp120 as evidenced by the K_D values for $[_{24}GQTL_{27}]CT = 207\ \mu M$ (*18*) versus $[_{20}GQTL_{23}]ST = 132\ \mu M$ (data not shown). Hence, for the current investigation, EGLV, the most frequently selected sequence from the phage library, was synthesized in the ST scaffold, yielding $[_{20}EGLV_{23}]ST$.

sCD4 Competition. When bound to phage, $[_{24}EGLV_{27}]CT$ was competed most effectively by sCD4 (*18*). To verify that the binding of soluble peptides to gp120 is competed by sCD4 in the same manner as phage-bound peptides were competed, an assay measuring sCD4 competition was initiated. The soluble peptide $[_{20}EGLV_{23}]ST$ (in the scyllatoxin scaffold, outlined above) was examined for its ability to compete with immobilized sCD4 by optical biosensor analysis (Figure 1a). When compared to gp120 alone, the presence of $[_{20}EGLV_{23}]ST$ decreased gp120 binding to sCD4 in a manner similar to $[_{20}AGSF_{23}]ST$ (Figure 1b), indicating that $[_{20}EGLV_{23}]ST$ binds to gp120 competitively with CD4. These data indicate that the soluble peptide behaves in a manner similar to the phage-bound peptide extracted from the original library.

Binding of CD4 Mimetic Peptides to YU2 gp120. The optical biosensor was used to measure the affinity of gp120 for $[_{20}EGLV_{23}]ST$ and $[_{20}AGSF_{23}]ST$ by direct binding of peptides as analytes to immobilized YU2. The YU2 gp120 binding affinities obtained by the biosensor were 0.123 μM for $[_{20}AGSF_{23}]ST$ and 35.90 μM for $[_{20}EGLV_{23}]ST$ (Table 1). Sensorgrams of the peptides binding to YU2 gp120, however, showed evidence of possible peptide aggregation on the sensor surface as judged by the deviation of the data points from a 1:1 interaction model at higher peptide concentrations. To verify the affinity measurements made by the biosensor, isothermal titration calorimetry (ITC) was employed. ITC measures the interaction between two proteins (or peptides) in solution by recording the amount of heat generated upon binding. The results found by ITC and optical biosensor were compared because these techniques use alternate approaches when measuring affinity. The binding affinities for the ST peptides to YU2 gp120 by isothermal titration calorimetry were 0.12 and 15.2 μM for $[_{20}AGSF_{23}]ST$ and $[_{20}EGLV_{23}]ST$, respectively (Table 1). The affinity values obtained by the two methods are very similar, indicating that the perceived aggregation did not have a significant effect on the estimates of binding affinity.

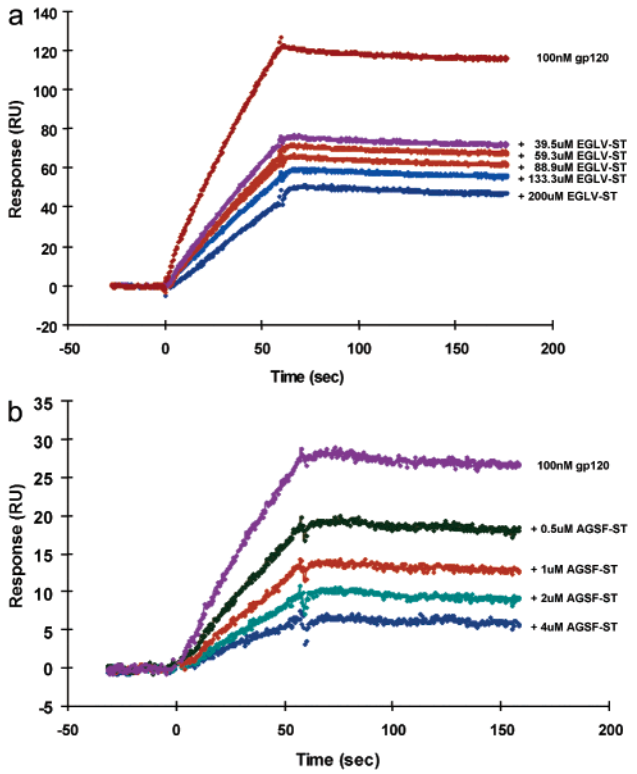

FIGURE 1: Competition of sCD4 for gp120 binding by mimetic peptides. With sCD4 immobilized on the sensor chip surface, solutions of gp120 (100 nM) with or without mimetic peptide are passed over the sensor chip and binding is recorded. (a) Added concentrations of $[_{20}EGLV_{23}]ST$ (39.5−200 μM) to gp120 decrease the binding of gp120 to the sCD4 surface progressively. (b) Similarly, the presence of $[_{20}AGSF_{23}]ST$ (0.5−4 μM) decreases the binding of gp120 to sCD4. The peptides (alone) did not show binding to the sCD4 surface (data not shown). These results indicate a competitive relationship between sCD4 binding to gp120 versus peptide binding to gp120.

Table 1: Binding Affinities of CD4 Mimetic Peptides to gp120 as Measured by Biosensor (surface plasmon resonance, SPR) and Isothermal Titration Calorimetry (ITC)

peptide	SPR (μM)	ITC (μM)
$[_{20}AGSF_{23}]ST$	0.123 ± 0.018	0.12 ± 0.02
$[_{20}EGLV_{23}]ST$	35.90 ± 6.55	15.2 ± 1.5

Effect of CD4 Mimetic Peptides on YU2 gp120 Binding to 17b. To examine the effect of the nonaromatic peptide on gp120 binding to 17b, a three-component optical biosensor assay was used (*14*). When compared with gp120 alone, the presence of $[_{20}EGLV_{23}]ST$ enhances the binding of gp120 to 17b Fab (Figure 2a). This effect is similar to that found with $[_{20}AGSF_{23}]ST$ (Figure 3a) and with the effects of sCD4 and our original CD4 mimetic peptide TXM1, or $[_{24}QGSF_{27}]$-CT (*14*). From these data, it is evident that an aromatic residue in the mimetic peptides is not required to enhance gp120 binding to 17b.

To quantify the extent of peptide enhancement of 17b binding by gp120, the kinetic parameters for each peptide−gp120 complex were examined. This analysis focused on on-rate comparisons. The off-rate of each complex, while measurable by optical biosensor, is a composite of several processes and only reports the slowest step. The off-rate can include dissociation of the gp120−peptide complex from 17b, dissociation of the peptide from gp120, and, possibly,

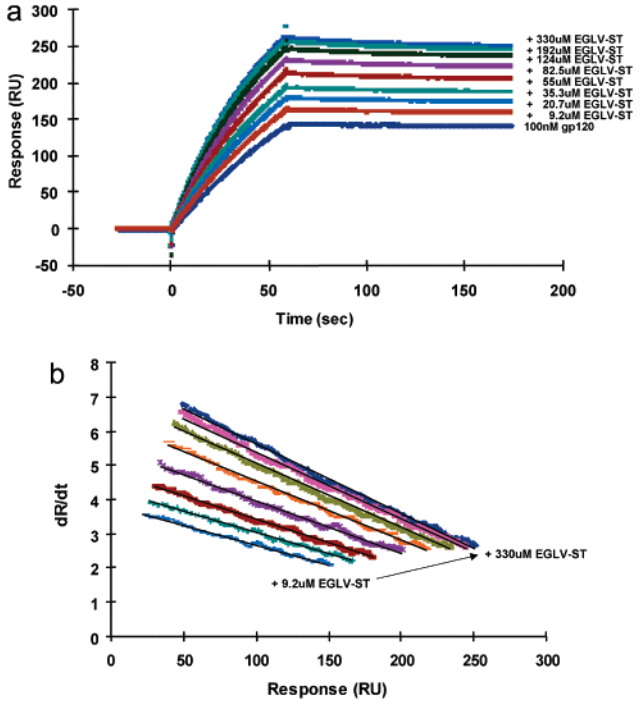

FIGURE 2: Effect of [$_{20}$EGLV$_{23}$]ST on gp120 binding to 17b. (a) With 17b Fab immobilized to the sensor chip, solutions of gp120 (100 nM) with or without [$_{20}$EGLV$_{23}$]ST were passed over the sensor chip. As the amount of peptide increased (9.2−330 μM), the binding of gp120 to 17b Fab also increased. [$_{20}$EGLV$_{23}$]ST (alone) did not bind to the 17b Fab surface (data not shown). (b) The association phase of the sensorgrams are plotted as the derivative (dR/dt) versus response (R). Each set of data corresponds to a single concentration measurement (in duplicate). The slopes of these lines (found by linear regression shown in black) are used in the $-ks$ plots (Figure 4).

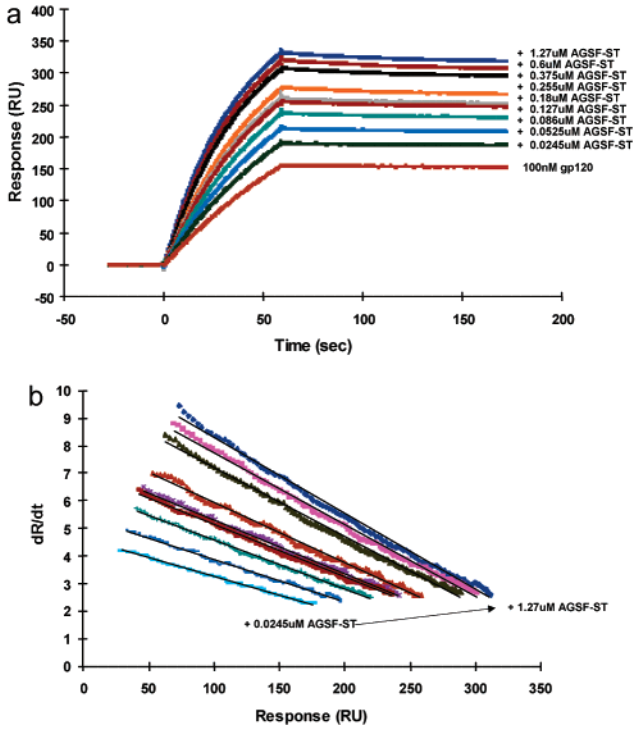

FIGURE 3: Effect of [$_{20}$AGSF$_{23}$]ST on gp120 binding to 17b. (a) With 17b Fab immobilized to the sensor chip, solutions of gp120 (100 nM) with or without [$_{20}$AGSF$_{23}$]ST were passed over the chip. As the amount of [$_{20}$AGSF$_{23}$]ST increased (0.025−1.27 μM), binding between gp120 and 17b also increased. [$_{20}$AGSF$_{23}$]ST (alone) did not bind to the 17b Fab surface (data not shown). (b) The association of the [$_{20}$AGSF$_{23}$]ST−gp120 complex can be plotted as the derivative. Each set of data corresponds to one concentration (in duplicate except for 0.255 and 0.18 μM [$_{20}$AGSF$_{23}$]-ST). Linear regression (black lines) reveals the slopes of these lines, which are used in the $-ks$ plots (Figure 4).

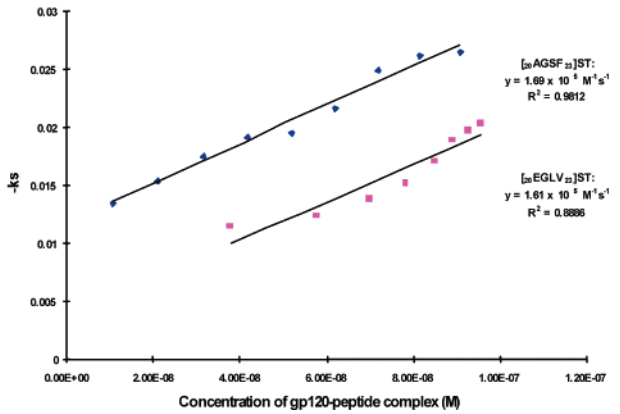

FIGURE 4: Calculation of the apparent on-rates for binding of the peptide−gp120 complexes to 17b. The slopes of the dR/dt plots (Figures 2b and 3b) are plotted versus concentration of peptide−gp120 complex. This concentration is based on the K_D for gp120 and each peptide from ITC. Slopes of the lines in the current plot reveal the apparent on-rates for the complexes. The [$_{20}$AGSF$_{23}$]-ST−gp120 complex (◆, diamonds) has an apparent on-rate of 1.69 × 10^5 M^{-1} s^{-1}. This value is very similar to the apparent on-rate for the [$_{20}$EGLV$_{23}$]ST-gp120 complex (■, squares), 1.61 × 10^5 M^{-1} s^{-1}, indicating that there is no difference in on-rate between the complex containing a peptide with a Phe ([$_{20}$AGSF$_{23}$]ST) versus that without a Phe ([$_{20}$EGLV$_{23}$]ST).

dissociation of uncomplexed gp120 from 17b. Thus, the dissociation data were not considered to be reliable indicators of off-rates of the gp120−peptide complexes from 17b and were not included in the evaluation.

To evaluate the on-rate processes for binding of each peptide−gp120 complex to the 17b Fab surface, the association data from Figures 2a and 3a were plotted in the form of dR/dt vs R (Figures 2b and 3b, respectively), and k_s values were determined by linear regression. The concentration of peptide−gp120 complex was calculated based on the amounts of each species present and the K_D of the interaction between the two molecules as measured by ITC. These values were plotted versus $-k_s$ of the interaction of the complex with 17b Fab (Figure 4). In this way, the on-rate data for gp120−peptide binding to immobilized 17b is normalized to account for differences in affinity for gp120 between [$_{20}$AGSF$_{23}$]ST (i.e., with an aromatic residue) and [$_{20}$EGLV$_{23}$]ST (i.e., without an aromatic residue). Linear regression of the data from Figure 4 yields the on-rate of the interaction from the slope of the regression line. The $-k_s$ plot of the [$_{20}$EGLV$_{23}$]-ST−gp120 complex gives an apparent on-rate of 1.61 × 10^5 M^{-1} s^{-1}, which is only slightly different than the apparent on-rate for [$_{20}$AGSF$_{23}$]ST−gp120, 1.69 × 10^5 M^{-1} s^{-1} (Figure 4).

Effect of F43V (D1D2) sCD4 and D1D2 sCD4 on YU2 gp120 Binding to 17b. The apparent noninvolvement of the peptide β-loop aromatic residue in the activation of gp120 binding to 17b led us to examine the effect of replacing the Phe43 side chain in sCD4 D1D2. F43V (D1D2) sCD4 was compared with D1D2 sCD4 in the 17b three-component optical biosensor assay. When compared with gp120 alone, the presence of F43V sCD4 enhances the binding of gp120

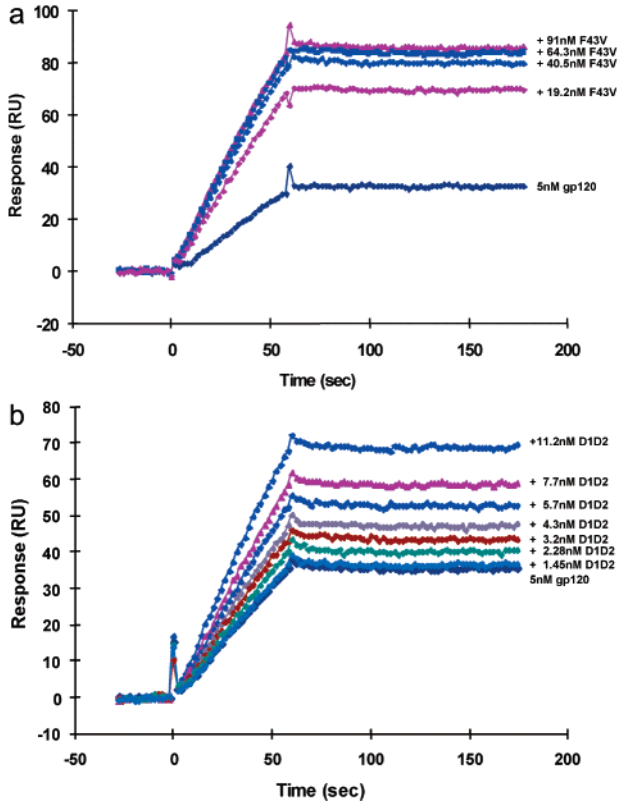

FIGURE 5: Effect of F43V (D1D2) sCD4 and D1D2 sCD4 on gp120 binding to 17b. With 17b Fab immobilized to the sensor chip, solutions of gp120 (5 nM) with or without sCD4-related protein were passed over the surface. (a) Addition of F43V (D1D2) sCD4 (19.2−91.0 nM) to gp120 shows an enhancement of binding between gp120 and 17b. (b) Similarly, D1D2 sCD4 (1.45−11.2 nM) enhances the binding of gp120 to 17b. These results show that the Phe of sCD4 is not necessary to increase 17b binding by gp120.

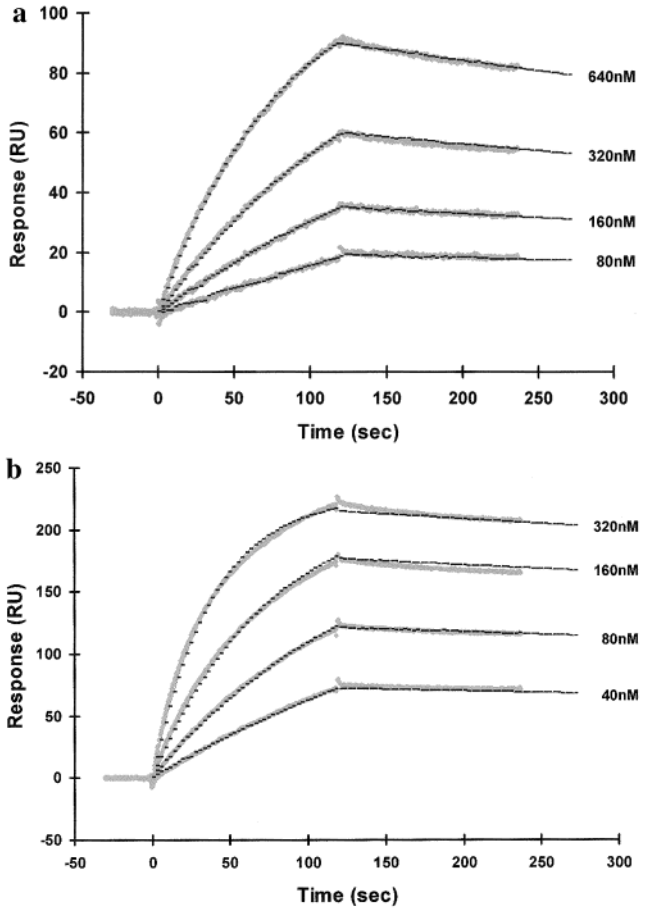

FIGURE 6: Binding of F43V (D1D2) sCD4 and D1D2 sCD4 to gp120. With gp120 immobilized on the sensor chip, increasing concentrations of F43V or D1D2 were passed over the chip. (a) Addition of increasing amounts of F43V to the gp120 surface resulted in a dose-dependent increase in binding signal. Global fitting of the binding data (black lines) between F43V and gp120 resulted in a K_D of 35 nM. (b) Binding of D1D2 sCD4 to gp120 resulted in a K_D of 4.3 nM by global fitting the data (black lines).

to 17b Fab (Figure 5a). This effect is similar to that seen with D1D2 sCD4 (Figure 5b). From these results, it can be concluded that the CDR2 β-turn aromatic residue in sCD4 is not required to enhance the binding of gp120 to 17b.

We next compared on-rates of D1D2 sCD4−gp120 complexes to 17b, as done for the peptide−gp120 complexes above. We first obtained firm values for the affinity between YU2 gp120 and both F43V (D1D2) sCD4 and D1D2 sCD4. These parameters had been measured for BH10 gp120 and found to be 1.9 nM and 360 nM for D1D2 and F43V sCD4, respectively, a difference of 190-fold between the wild-type and mutant proteins (*16*). The affinities of these D1D2 sCD4 proteins for YU2 gp120 were measured in the current study using optical biosensor analysis (Figure 6). After applying a 1:1 Langmuir binding model (global fit), the K_D values derived were 4.5 and 35 nM for D1D2 and F43V, respectively, a difference of 7.8-fold (a differential smaller than that found with BH10 gp120 but still substantial). For comparison, full-length sCD4 was analyzed in the same binding assay and found to have a K_D value of 4.3 nM for YU2 gp120 (data not shown). This value agrees with results from prior studies which found equivalent affinities for full-length versus D1D2 sCD4 (*16*).

Using the above K_D values for gp120 binding to the sCD4 D1D2 forms, the $-k_s$ values for both sCD4 proteins were calculated and plotted by the same procedure used for the peptides (see above, Figure 4). The F43V sCD4−gp120 complex gives an apparent on-rate of 4.7×10^5 M^{-1} s^{-1} when binding to 17b (Figure 7). This value is indistinguishable from the apparent on-rate for the 17b interaction with wild-type D1D2 sCD4−gp120 complex, 4.9×10^5 M^{-1} s^{-1} (Figure 7).

Effect of CD4 Mimetic Peptides on YU2 gp120 Binding to CCR5$^+$ Cells. The above experiments demonstrated that the aromatic residue in the β-turn binding epitope of both sCD4 D1D2 and CD4-mimetic ST peptides is not required for upregulating 17b binding by gp120. We then turned to the question of the role of the aromatic residue in upregulating co-receptor binding in cells. Previous experiments showed that sCD4 itself induced increased binding of gp120 to cell-bound co-receptor. Hence, we here examined the effect with mimetic peptides. [$_{20}$EGLV$_{23}$]ST and [$_{20}$AGSF$_{23}$]-ST were each combined with gp120, and binding of the resulting complexes to CCR5−Cf2 cells was measured. The results (Figure 8) show that both peptides activate gp120 toward CCR5 binding when compared with a non-gp120 binding peptide. Further, the effects of these peptides are equivalent when viewed at their respective K_D values. Addition of [$_{20}$EGLV$_{23}$]ST or [$_{20}$AGSF$_{23}$]ST did not enhance the binding of YU2 gp120 to CXCR4$^+$ cells (data not shown). These results, taken with the results from the three-

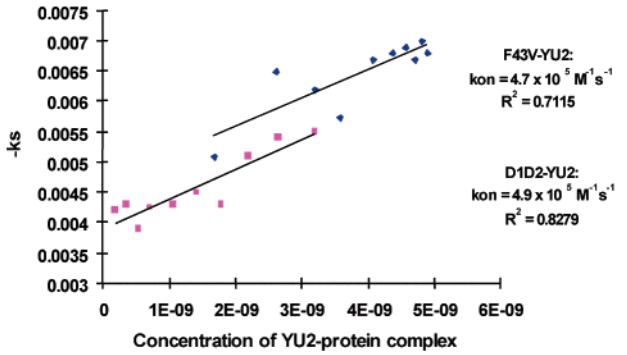

FIGURE 7: Optical biosensor determination of apparent on-rates for binding of F43V sCD4−gp120 and D1D2 sCD4−gp120 complexes to 17b. The analyses were carried out in the same manner as for the mimetic peptides (Figure 4). Primary data were collected for F43V sCD4 (91−1450 nM) and D1D2 sCD4 (0.35−1.45 nM) binding to immobilized YU2 using the same sensor chip as in Figure 5. Slopes of the d*R*/d*t* plots of association data were plotted versus the concentration of the sCD4 protein−gp120 complex. The amount of complex was calculated based on the added concentrations of reactants and their measured K_D values (from the data of Figure 6). Binding of the F43V−gp120 complex to 17b results in an apparent on-rate of 4.7×10^5 M^{-1} s^{-1}. This value is nearly identical to that found for the apparent on-rate for the D1D2−gp120 complex, 4.9×10^5 M^{-1} s^{-1}.

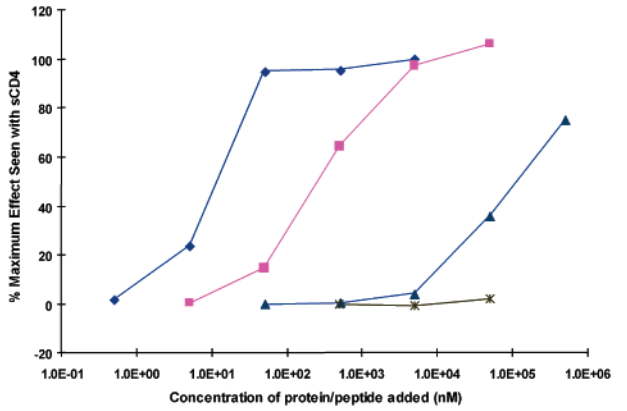

FIGURE 8: Effect of mimetic peptides on gp120 binding to $CCR5^+$ cells. gp120 binding to $CCR5^+$ cells was measured using C11 antibody/IgG-PE detection. gp120 binding alone is plotted as the zero (0) point. sCD4 (◆), $[_{20}AGSF_{23}]ST$ (■), and $[_{20}EGLV_{23}]ST$ (▲) were added to gp120 (at the concentrations indicated) and binding to $CCR5^+$ cells was again measured. Plotted are the effects of the peptides as a percent of the measured maximal sCD4 effect. Also plotted are the data for a peptide that does not bind to gp120, used as a negative control (∗). From this, it is clear that the two ST peptides (with and without a Phe) can enhance the binding of gp120 to CCR5. Also, it is clear that the difference in efficacy between the two peptides could be entirely related to the difference in their gp120 binding abilities.

component 17b biosensor kinetics assay, argue that an aromatic residue in itself is not required to activate the co-receptor/17b binding site in the envelope protein.

DISCUSSION

In the present study, we used miniprotein mimetics to examine structural elements in CD4 that are important for inducing cooperative upregulation of the 17b/co-receptor recognition site in HIV-1 env. Prior results with an epitope-randomized sequence library based on phage-displayed scorpion toxin peptide (CT) revealed gp120-binding epitopes that contain neither a Phe residue nor any other aromatic residue. In view of the known importance of CD4's Phe43 as a key part of the binding epitope for HIV-1 env gp120, we asked what role an aromatic residue plays in the mechanism of CD4 binding to gp120 and consequent gp120 activation toward chemokine receptor binding. In this paper, we have shown that CD4 proteins and CD4-mimetic synthetic peptides lacking a phenylalanyl side chain in the β-turn binding epitope enhance binding of gp120 to 17b in a manner similar to that of corresponding Phe-bearing ligands. Upon quantifying these 17b binding enhancements, no difference was observed in the apparent association rate of 17b binding between the $[_{20}EGLV_{23}]ST$−gp120 and the $[_{20}AGSF_{23}]ST$−gp120 complexes, or between F43V sCD4−gp120 and D1D2 sCD4−gp120 complexes. The results show that, while the Phe- and Val-containing ligands have differential affinities for gp120, their induction of gp120 binding to 17b are the same. Furthermore, we were able to show equally comparable effects of Phe- vs Val-containing peptides on binding of gp120 to cell-displayed co-receptor CCR5.

The importance of a Phe residue in the CDR2 β-turn of CD4 to stabilize binding to gp120 has been reiterated many times, through site-directed mutagenesis, crystallography, and protein−protein interaction studies (*15*−*17*). Because of this, the phenylalanine side chain has been a central focus in the design of CD4 mimetic peptides. Consistently, Val replacement of Phe in $[_{20}EGLV_{23}]ST$ leads to lower affinity than the similar $[_{20}AGSF_{23}]ST$. Yet, $[_{20}EGLV_{23}]ST$ nonetheless appears to bind in a distinctly CD4-like manner as judged by the positive 17b effect, arguing that loss of the Phe side chain on its own does not remove CD4-like stabilizing contacts. One possible explanation for this is that the Val side chain, or possibly that of the Leu next to it, could replace the Phe side chain the "Phe43 cavity" of gp120 (*15*). Stabilizing interactions might be reduced but not lost by such a substitution. Docking studies are currently in progress to evaluate the potential impact of Phe replacement on miniprotein mimetic-gp120 interaction (J. LaLonde, M. Head, and C. Peishoff, personal communication).

A consistent observation of this work is that the aromaticity of the Phe residue in the CDR2 β-turn of CD4 and in the corresponding epitope of mimetic scorpion toxin peptides appears differentially more critical for affinity than for 17b/coreceptor site activation. This differential effect of Phe-to-Val replacement suggests the possibility that the structural components of CD4 for stabilizing gp120 binding vs activation of the gp120 binding site for 17b/co-receptor may in fact be different. This in turn suggests that peptide mimetic design at and around the β-turn Phe epitope may be controlled to differentially effect gp120 affinity vs co-receptor binding site accessibility. This evokes the intriguing, but as yet unachieved, possibility of designing or otherwise discovering "nonactivating miniprotein antagonists", namely CD4-mimicking ligands which could bind in the CD4 binding site of env without activating the co-receptor site. This possibility is supported by structure-based thermodynamic analysis of the sCD4/gp120 interaction using the CORE_BIND algorithm (see references *28*−*30* for details). CORE_BIND calculates the propagation of the binding energy from the contact region to the rest of the protein. When applied to the sCD4/gp120 structure, a cooperative path that connects the sCD4 and co-receptor binding site

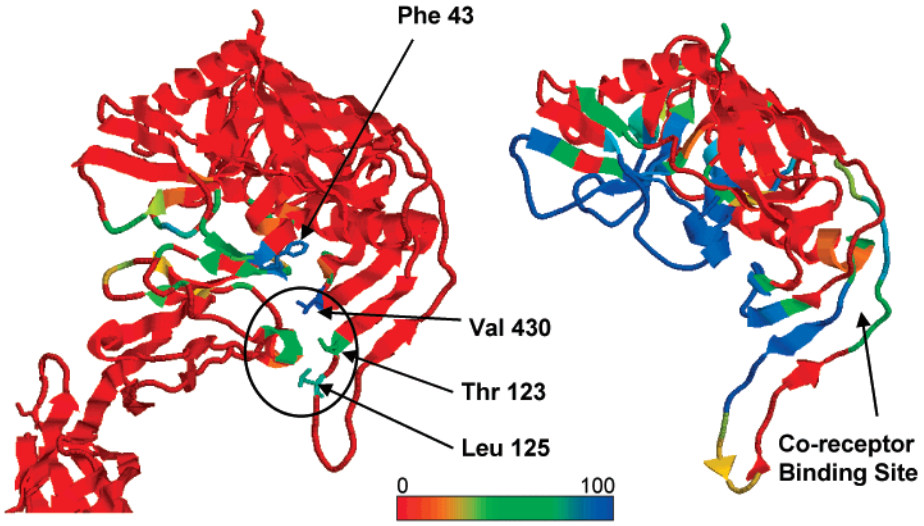

FIGURE 9: (Left panel) Binding interface between sCD4 and gp120 color coded according to the contributions of specific residues to the binding affinity. A rainbow color scale in which red indicates no contribution and blue maximal contribution has been used. Shown in stick representations are Phe43 in sCD4 and Thr123, Leu125 and Val430 in gp120. Most of the binding affinity is concentrated around Phe43 and adjacent areas. (Right panel) The structure of gp120 showing the propagation of the binding energy throughout its three-dimensional structure. In this figure a rainbow color scale in which blue denotes maximal effect and red no effect has been used. Val430, Thr123 and Leu125 appear to be key residues for the initiation of the cooperative effect that propagates through the β sheet and V1/V2 loop and leads to the structural stabilization of the co-receptor site. The structure-based thermodynamic analysis was performed as described in ref *29*.

becomes apparent. The gp120 amino acids that define the binding site for sCD4 are structurally stabilized in their bound conformation as a result of their interactions with sCD4. Because the residues at the binding site also interact with other residues in gp120, this stabilization propagates to distal regions. This propagation is, however, not uniform and affects specific sets of residues in different manners. The results of this analysis are shown in Figure 9. The left panel highlights the protein regions that contribute the most to the binding affinity. This figure uses a rainbow scale in which blue indicates the residues that contribute the most and red the least. The binding interface is extensive and buries from the solvent a surface area close to 2000 Å^2 (*15*). The binding energy, however, is not distributed uniformly throughout this interface. Some residues are predicted to contribute significantly to the binding affinity, notably the region around Phe43 (shown in a stick representation as a reference point). While the interactions around Phe43 are critical for binding affinity, the results in this paper indicate that a miniprotein lacking the critical Phe residue binds with an expected lower affinity but is still able to trigger a cooperative response, suggesting other possible paths for the allosteric stabilization of the co-receptor site. The right panel illustrates the expected propagation of the binding energy throughout the gp120 structure. As expected, the binding site itself is significantly stabilized (blue). However, the structural stabilization is not limited to the gp120 residues in immediate contact with sCD4 but propagates away from the binding site. In particular, the results indicate that the stabilization of the co-receptor site involves primarily the interactions of sCD4 with the bridging β-sheet rather than the interactions that originate at the Phe43 site. Figure 9 highlights three residues Val430, Thr123, and Leu125 in gp120 that interact directly with sCD4 and could provide an anchoring point for sCD4 to the bridging β sheet and the V1/V2 loop. Thr123 is expected to have the largest cooperative effect due to its location directly in the bridging β sheet. Leu125, at the tip of the V1/V2 loop, elicits the smallest effect as shown in the figure. These conclusions are in agreement with recent experimental observations that link mutations in the bridging β sheet to an impaired neutralization sensitivity of gp120 (*31*). Also, a mutation in Thr123 was shown to have little effect on CD4 binding but significantly decreased chemokine receptor binding (*11*). Together, the results presented in this paper point to an intriguing hypothesis, that those residues that contribute the most to the binding affinity, the so-called binding hot spots (e.g., the region around Phe43), are not necessarily the same as those that are critical for the cooperative propagation of binding effects and that they are not required to overlap structurally.

The question of which set of residues in CD4 is most responsible for promoting gp120 conformational change and consequent co-receptor site activation is still unresolved by direct mutagenic analysis. It has been shown previously that CD4 binding induces movement of the V1/V2 loops in gp120, which contributes to exposure of the 17b/CCR5 binding sites (*32*, *33*). Structurally minimized CD4 mimetics, such as the ST variants of the current study, clearly carry many of the structural elements needed for activation of 17b/co-receptor binding. Hence, further mutagenic analysis with these mimetics offers a potentially important means to help delineate the co-receptor site activation epitopes of CD4.

An important finding from this study is that the increase in gp120 binding to 17b due to the presence of the CD4 mimetic peptides is the same as the increase in binding seen between gp120 and CCR5$^+$ cells when these peptides are present. The similarity of the effects of these two peptide−gp120 complexes on both CCR5 and 17b binding is consistent with the view that the 17b and CCR5 binding surfaces on gp120 are not greatly different. This result, in combination with prior epitope mapping and mutagenesis studies, validates the use of 17b binding as a model for CCR5 receptor binding, and hence the utility of the 17b assay as a convenient means to track structural elements in CD4 (as well as in gp120) which drive activation of binding of the HIV-1 envelope to the host cell co-receptor.

Although the wild-type CD4 sequence, QGSF, was among the frequently selected sequences from the phage library, neither it nor other sequences containing aromatic residues was the most frequently selected. One might wonder why phage selection, which is based on gp120 binding, resulted predominantly in hydrophobic but nonaromatic sequences, even though such sequences were found to lead to weaker gp120 affinity than the aromatic sequences when tested with isolated synthetic peptides. There are several reasons that could contribute to this result. It is possible that phage-bound peptides bind to a site on gp120 that is not precisely equivalent to the site occupied by CD4 or by soluble synthetic peptides. A completely different binding site for the two entities is unlikely given our competition ELISA (*18*) and biosensor results. However, small changes in the binding site location might be responsible for the preference of nonaromatic residues. In addition, it is possible that phage viability or expression levels are altered in the presence of certain peptides. These factors would alter the population of peptides available for binding. Nonetheless, it should be borne in mind that CD4 mutants where Phe43 is replaced by Leu, Val, and Ala, bind with significant affinity (*16*) to gp120, indicating that these hydrophobic, nonaromatic residues are acceptable binders for gp120.

In conclusion, while the residues involved in CD4−gp120 binding have been clearly defined by a number of methods, the structural elements required for triggering gp120 conformational change remain elusive. We believe that continued exploration of CD4 mimetic peptides, coordinately with sCD4 mutagenesis, will provide an effective means to further clarify residues that influence CD4−gp120 binding vs gp120 activation. Defining these structural elements hopefully can give insight into the mechanism of host cell entry by HIV-1, as well as lead to progress in the design of entry antagonists.

ACKNOWLEDGMENT

We thank Drs. Wayne Hendrickson and Peter Kwong (Columbia University) for helpful discussions during the course of this work, Drs. Judith LaLonde, Martha Head and Catherine Peishoff (Glaxo SmithKline, Inc.) for discussion of their preliminary docking studies and Dr. Alyssa Biorn (UPenn) for thorough reading of the manuscript.

REFERENCES

1. Barre-Sinoussi, F., Chermann, J. C., Rey, F., Nugeyre, M. T., Chamaret, S., Gruest, J., Dauguet, C., Axler-Blin, C., Vezinet-Brun, F., Rouzioux, C., Rozenbaum, W., and Montagnier, L. (1983) *Science 220*, 868−71.
2. Sattentau, Q. J., and Moore, J. P. (1991) *J. Exp. Med. 174*, 407−15.
3. Sattentau, Q. J., Moore, J. P., Vignaux, F., Traincard, F., and Poignard, P. (1993) *J. Virol. 67*, 7383−93.
4. Choe, H., Farzan, M., Sun, Y., Sullivan, N., Rollins, B., Ponath, P. D., Wu, L., Mackay, C. R., LaRosa, G., Newman, W., Gerard, N., Gerard, C., and Sodroski, J. (1996) *Cell 85*, 1135−48.
5. Alkhatib, G., Combadiere, C., Broder, C. C., Feng, Y., Kennedy, P. E., Murphy, P. M., and Berger, E. A. (1996) *Science 272*, 1955−8.
6. Deng, H., Liu, R., Ellmeier, W., Choe, S., Unutmaz, D., Burkhart, M., Di Marzio, P., Marmon, S., Sutton, R. E., Hill, C. M., Davis, C. B., Peiper, S. C., Schall, T. J., Littman, D. R., and Landau, N. R. (1996) *Nature 381*, 661−6.
7. Doranz, B. J., Rucker, J., Yi, Y., Smyth, R. J., Samson, M., Peiper, S. C., Parmentier, M., Collman, R. G., and Doms, R. (1996) *Cell 85*, 1149−58.
8. Dragic, T., Litwin, V., Allaway, G. P., Martin, S. R., Huang, Y., Nagashima, K. A., Cayanan, C., Maddon, P. J., Koup, R. A., Moore, J. P., and Paxton, W. A. (1996) *Nature 381*, 667−73.
9. Connor, R. I., Sheridan, K. E., Ceradini, D., Choe, S., and Landau, N. R. (1997) *J. Exp. Med. 185*, 621−8.
10. Berger, E. A., Murphy, P. M., and Farber, J. M. (1999) *Annu. Rev. Immunol. 17*, 657−700.
11. Rizzuto, C. D., Wyatt, R., Hernandez-Ramos, N., Sun, Y., Kwong, P. D., Hendrickson, W. A., and Sodroski, J. (1998) *Science 280*, 1949−53.
12. Mondor, I., Moulard, M., Ugolini, S., Klasse, P. J., Hoxie, J., Amara, A., Delaunay, T., Wyatt, R., Sodroski, J., and Sattentau, Q. J. (1998) *Virology 248*, 394−405.
13. Trkola, A., Drajic, T., Arthos, J., Binley, J., Olson, W., Allaway, G., Cheng-Mayer, C., Robinson, J., Maddon, P., and Moore, J. (1996) *Nature 384*, 184−7.
14. Zhang, W., Canziani, G., Plugariu, C., Wyatt, R., Sodroski, J., Sweet, R., Kwong, P., Hendrickson, W., and Chaiken, I. (1999) *Biochemistry 38*, 9405−16.
15. Kwong, P. D., Wyatt, R., Robinson, J., Sweet, R. W., Sodroski, J., and Hendrickson, W. A. (1998) *Nature 393*, 648−59.
16. Wu, H., Myszka, D. R., Tendian, S. W., Brouillette, C. F., Sweet, R. W., Chaiken, I. M., and Hendrickson, W. A. (1996) *Proc. Natl. Acad. Sci. U.S.A. 93*, 15030−5.
17. Moebius, U., Clayton, L. K., Abraham, S., Harrison, S. C., and Reinherz, E. L. (1992) *J. Exp. Med. 176*, 507−17.
18. Li, C., Dowd, C. S., Zhang, W., and Chaiken, I. M. (2001) *J. Pept. Res. 57*, 507−18.
19. Vita, C., Drakopoulou, E., Vizzavona, J., Rochette, S., Martin, L., Menez, A., Roumestand, C., Yang, Y. S., Ylisastigui, L., Benjouad, A., and Gluckman, J. C. (1999) *Proc. Natl. Acad. Sci. U.S.A. 96*, 13091−6.
20. Ferrer, M., and Harrison, S. C. (1999) *J. Virol. 73*, 5795−802.
21. Chen, S., Chrusciel, A., Nakanishi, H., Raktabutr, A., Johnson, M. E., Sato, A., Weiner, D., Hoxie, J., Saragovi, H. U., Greene, M. I., and Kahn, M. (1992) *Proc. Natl. Acad. Sci. U.S.A. 89*, 5872−6.
22. Darbon, H., Blanc, E., and Sabatier, J.-M. (1999) *Perspect. Drug Discovery Des. 15/16*, 41−60.
23. Bontems, F., Roumestand, C., and Gilquin, B. (1991) *Science 254*, 1521−3.
24. Culp, J. S., Johansen, H., Hellmig, B., Beck, J., Matthews, T. J., Delers, A., and Rosenberg, M. (1991) *Biotechnology 9*, 173−7.
25. Willey, R. L., Martin, M. A., and Peden, K. W. (1994) *J. Virol. 68*, 1029−39.
26. Vita, C., Bontems, F., Bouet, F., Tauc, M., Poujeol, P., Vatanpour, H., Harvey, A. L., Menez, A., and Toma, F. (1993) *Eur. J. Biochem. 217*, 157−69.
27. Babcock, G. J., Mirzabekov, T., Wojtowicz, W., and Sodroski, J. (2001) *J. Biol. Chem. 276*, 38433−40.
28. Luque, I., and Freire, E. (2000) *Proteins (Suppl.) 4*, 63−71.
29. Freire, E. (1999) *Proc. Natl. Acad. Sci. U.S.A. 96*, 10118−22.
30. Freire, E. (2000) *Proc. Natl. Acad. Sci. U.S.A. 97*, 11680−2.
31. Zhu, C., Zhu, L., Holz-Smith, S., Matthews, T., and Chen, C. (2001) *Proc. Natl. Acad. Sci. U.S.A. 98*, 15227−32.
32. Wyatt, R., Moore, J., Accola, M., Desjardin, E., Robinson, J., and Sodroski, J. (1995) *J. Virol. 69*, 5723−33.
33. Kolchinsky, P., Kiprilov, E., Bartley, P., Rubinstein, R., and Sodroski, J. (2001) *J. Virol. 75*, 3435−43.

BI012168I